POLITECNICO DI TORINO
Repository ISTITUZIONALE

Experimental and Modeling Study of Metal–Insulator Interfaces to Control the Electronic Transport in Single Nanowire Memristive Devices

(Article begins on next page)

29 November 2022

Research Article

Experimental and Modeling Study of Metal−Insulator Interfaces to Control the Electronic Transport in Single Nanowire Memristive Devices

Gianluca Milano,* Enrique Miranda, Matteo Fretto, Ilia Valov, and Carlo Ricciardi*

Cite This: https://doi.org/10.1021/acsami.2c11022

Read Online

ACCESS | Metrics & More | Article Recommendations | Supporting Information

ABSTRACT: Memristive devices relying on redox-based resistive switching mechanisms represent promising candidates for the development of novel computing paradigms beyond von Neumann architecture. Recent advancements in understanding physicochemical phenomena underlying resistive switching have shed new light on the importance of an appropriate selection of material properties required to optimize the performance of devices. However, despite great attention has been devoted to unveiling the role of doping concentration, impurity type, adsorbed moisture, and catalytic activity at the interfaces, specific studies concerning the effect of the counter electrode in regulating the electronic flow in memristive cells are scarce. In this work, the influence of the metal−insulator Schottky interfaces in electrochemical metallization memory (ECM) memristive cell model systems based on single-crystalline ZnO nanowires (NWs) is investigated following a combined experimental and modeling approach. By comparing and simulating the electrical characteristics of single NW devices with different contact configurations and by considering Ag and Pt electrodes as representative of electrochemically active and inert electrodes, respectively, we highlight the importance of an appropriate choice of electrode materials by taking into account the Schottky barrier height and interface chemistry at the metal−insulator interfaces. In particular, we show that a clever choice of metal−insulator interfaces allows to reshape the hysteretic conduction characteristics of the device and to increase the device performance by tuning its resistance window. These results obtained from single NW-based devices provide new insights into the selection criteria for materials and interfaces in connection with the design of advanced ECM cells.

KEYWORDS: metal−insulator interfaces, memristive devices, resistive switching, nanowires, schottky barriers
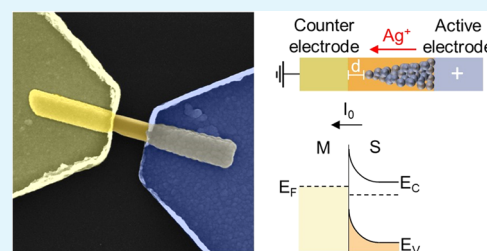
INTRODUCTION

Memristive technologies are considered promising candidates for the development of alternative memory devices for data storage and for the development of computing architectures beyond von Neumann architecture, paving the way for in-memory computing and neuromorphic systems.[1−11] Redox-based memristive devices are essentially two-terminal metal−insulator−metal cells in which the internal resistance state can be modulated by ionic effects under the action of an external electrical stimulation.[12−14] In particular, resistive switching mechanism underlaying memristive functionalities in electrochemical metallization cells (ECMs) relies on the formation/dissolution of a metallic filament that bridges the two electrodes.[15] In this case, a positive voltage applied to the electrochemically active electrode can cause the dissolution of metal atoms to form metal ions that start to migrate toward the counter electrode under the action of the applied electric field. This leads to the formation of a metallic filament after recrystallization, causing the switching of the memristive cell from a high-resistance state (HRS) to a low-resistance state (LRS). Depending on the operational conditions that control the lifetime of the metallic filament, the switching mechanism

in ECM cells can be either volatile or nonvolatile.[16−18] While nonvolatility represents a prerequisite for the development of memristive memories, great attention have been recently devoted to volatile devices that endow the capability of temporal processing of the input signal thus allowing the implementation of synaptic functionalities and unconventional computing paradigms.[19−23]

In the last years, important advancements in the understanding of the physicochemical processes regulating memristive dynamics and functionalities have been achieved. In this context, memristive devices based on nanowires (NWs) have demonstrated their suitability as model systems to investigate the intrinsic mechanism of switching in memristive cells by taking advantage of their planar structure and high localization
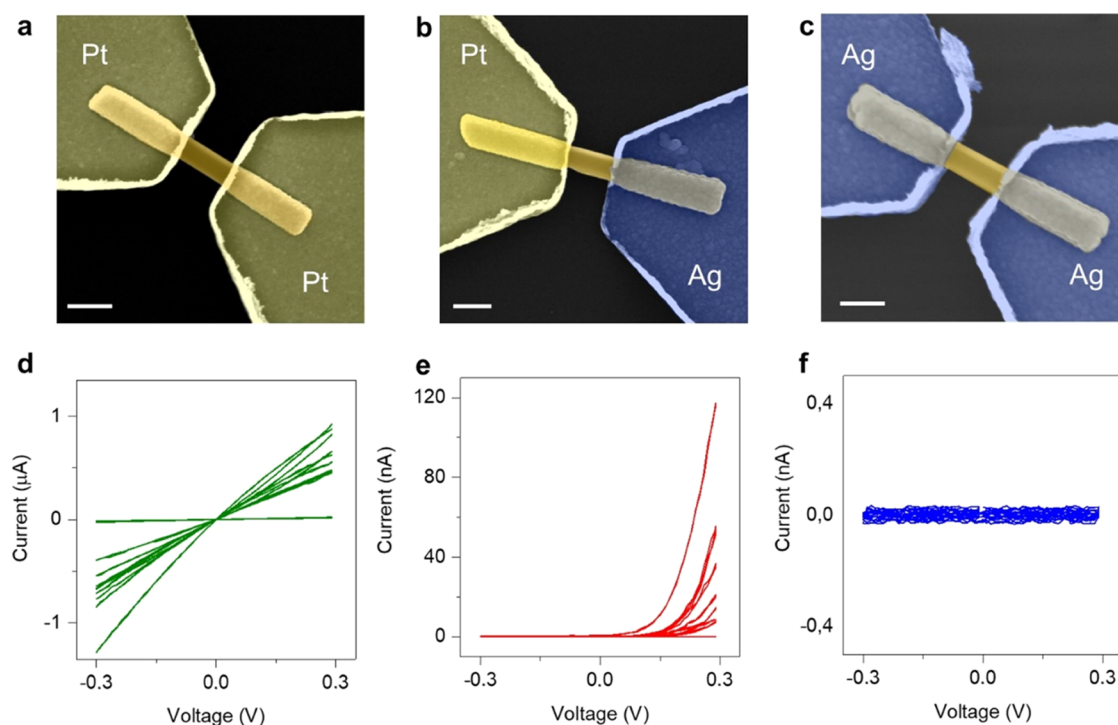
Figure 1. Single ZnO NW devices. Single NWs contacted by (a) symmetric Pt−Pt electrodes, (b) asymmetric Pt−Ag electrodes, and (c) symmetric Ag−Ag electrodes (scale bars, 250 nm) and corresponding I−V characteristics in the low-voltage range (panels d−f). For each electrode configuration, the electrical response of at least 10 different NW-based devices is reported.

of the switching events.[17,24−30] For redox-based switching devices, notable accomplishments have been reported in connection with half-cell redox reactions and nanoscale electrochemistry[31,32] together with new insights into the formation/dissolution of the filament by *in situ* and *ex situ* characterization techniques.[33−36] In addition, the impact of introducing dopants and impurities in the oxide matrix,[37] the influence of moisture,[38−41] and the combination of electrodes and electrolyte materials have been extensively investigated.[42] Importantly, significant interest has been devoted to the understanding of the role played by interfaces that, due to the nanoscale nature of the involved materials, can be more relevant in regulating the switching characteristic of the device than the active matrix itself.[43,44] Though not always explicitly discussed, the use of different electrodes and doping levels reflects in a change of the properties of interfaces that regulate both the ionic and the electronic flux. In valence change memories (VCMs), modifying the Schottky electrode−oxide interface using a variety of metal electrodes/oxides has been proposed as a way of altering the resistance of the cell.[43] Instead, while substantial efforts have been devoted to understand the influence of the catalytic activity of the counter electrode on the nanoionic processes taking place at the ECM cells,[45] studies on the influence of the counter electrode in the regulation of the electronic flux are scarce.

Here, we investigate through a combined experimental and modeling approach the role of metal−insulator interfaces in single-crystalline ZnO NW-based devices, used as memristive model systems. The influence of the metal−NW interface was analyzed by comparing devices with different metal electrodes both in symmetric and asymmetric configurations and by exploiting Ag and Pt as representative electrochemically active and inert metal electrodes, respectively. Besides comparing the influence of metal−NW interfaces in regulating the electronic

conduction mechanism in the pristine state, we show that interfaces can be appropriately tuned to modify the hysteretic behavior and the resistance window of the device. Within this framework, the crucial role of regulating the electronic conduction mechanism of the metal−insulator at the counter electrode is highlighted. In particular, it is shown that a proper choice of the counter electrode with a blocking character allows to reshape the hysteretic conduction characteristic and to enlarge the resistance window.

■ RESULTS AND DISCUSSION

Single NW memristive cells were realized by contacting single-crystalline and hexagonal-shaped ZnO NWs (diameter of ∼100 nm) grown by low-pressure chemical vapor deposition (LP-CVD) with metal electrodes through a combined optical and electron beam lithography (EBL), as detailed in our previous works[46−48] (details of the ZnO NW synthesis and device fabrication can be found in the Experimental Section). Concerning device scalability, it is worth noticing that the ZnO NW diameter can be further reduced by exploiting peculiar growth strategies that allows the growth of ZnO NWs with diameters below 10 nm, as for example reported by Yin et al.[49] that exploited a catalyst-assisted growth technique. The role of the metal−insulator interfaces on the electronic transport properties and switching behavior of single NW memristive cells was evaluated by exploiting Ag and Pt as representative electrochemically active and inert electrodes, respectively, both in symmetric and asymmetric configurations as discussed in the next section.

Metal−Insulator Interfaces and Electronic Transport Mechanisms. Representative scanning electron microscopy (SEM) images of single NW memristive cells with symmetric Pt electrodes, asymmetric Pt and Ag electrodes, and symmetric
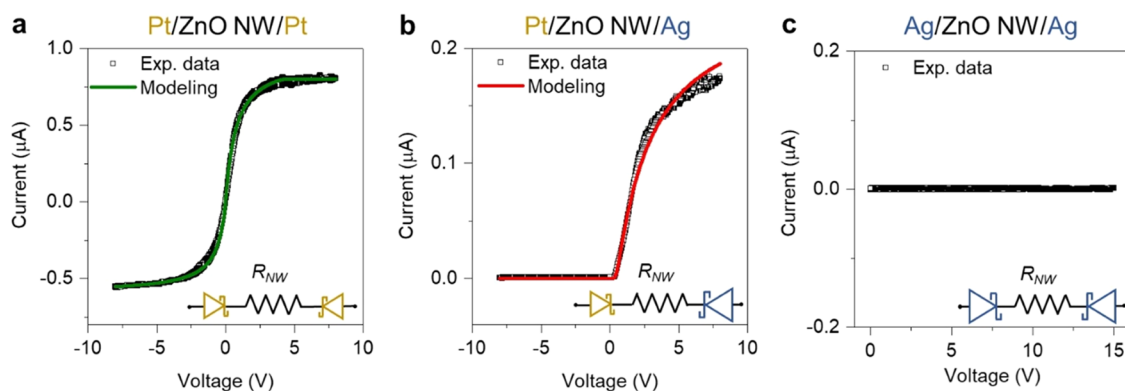
Figure 2. Experimental and modeling electronic transport properties of single ZnO NW devices in the pristine state. $I–V$ characteristics of ZnO NWs contacted with (a) symmetric Pt–Pt electrodes, (b) asymmetric Pt–Ag electrodes (positive voltage is applied to the Ag electrode), and (c) symmetric Ag–Ag electrodes. The equivalent circuital representations of devices represented by back-to-back connected Schottky junctions and the NW series resistance (R_{NW}) are reported as insets.

Ag electrodes are illustrated in Figure 1a–c, respectively. In the low-voltage range, symmetric Pt/ZnO NW/Pt devices yield an almost linear $I–V$ characteristic (Figure 1d), asymmetric Ag/ZnO NW/Pt devices resulted in a rectifying $I–V$ characteristic (Figure 1e), while symmetric Ag/ZnO NW/ZnO device resulted in a blocking characteristics (Figure 1f). Notably, the electrical characteristics of at least 10 devices for each configuration are reported in panels d–f of Figure 1 revealing that, despite device-to-device variability in current levels that can be ascribed to variations in contact geometries and junction areas,[50] comparable behavior is observed in different devices with the same electrode configuration. In this context, note also that small variations in nanosized contact geometries and junction areas at the two ends of the NW are responsible for nonperfectly symmetric $I–V$ characteristics of symmetric devices. The comparison of the pristine state electrical characteristics of NW-based devices contacted with different electrode configurations clearly demonstrates the influence of the metal–insulator interface in regulating the electronic conduction.

A combined experimental and modeling approach was exploited for a more detailed investigation of the role of metal–insulator interfaces on the electronic transport properties. In purely electronic transfer (i.e., without electrochemical reactions and ionic transport), the metal-insulating interface at the nanocontact can be modeled as a Schottky barrier, as a consequence of the semiconducting nature of the intrinsically n-type doped ZnO NWs.[51−54] In this case, electronic transport at the metal–ZnO interface of the nanocontact occurs through thermionic emission, where current can be phenomenologically expressed according to the relationship

$$I = I_0 \left[\exp\left(\frac{V}{\eta V_{\text{T}}} \right) - 1 \right] \tag{1}$$

where V is the applied voltage, I_0 is the inverse saturation current, η is the ideality factor, $V_{\text{T}} = kT/e$ is the thermal voltage at temperature T, k is the Boltzmann constant, and e is the electron charge. Note that the saturation current I_0 implicitly depends on the contact area, as well as on the Schottky barrier height, thus relying on the specific choice of the metal contact. Similarly, the ideality factor η representing the deviation of the electrical characteristics from the ideal thermionic emission theory relies on the specific metal considered for the contact. In this context, the pristine state

of the single ZnO NW memristive cell comprising two metal–ZnO interfaces can be electrically represented as two back-to-back connected Schottky barriers in series with the NW resistance, where each Schottky barrier is characterized by its particular value of I_0 and η. This electrical configuration does not have analytic solution for dissimilar devices, but it can be approximately solved using a piecewise model with nonlinear series resistance correction, as detailed in a previous work.[55] According to this simplified model and considering the impedance of the electrochemical reaction smaller than the Schottky barrier before electroforming, the voltage across the memristive cell can be simply expressed as

$$V = \pm \eta_{\text{L,R}} V_{\text{T}} \ln\left(\pm \frac{I}{I_{\text{0L,R}}} + 1 \right) + IR^{\pm} \tag{2}$$

where η_{L} and η_{R} are the ideality factors and I_{0L} and I_{0R} are the saturation currents of the two Schottky barriers, respectively. $R^{\pm}$ is an effective series resistance that endows the NW resistance (R_{NW}) and contact effects. + and − represent the sign of the applied voltage. From (2), the current flowing through a single NW device can be described by the more complex expression[55]

$$I^{\pm} = \pm \frac{\eta_{\text{L,R}} V_{\text{T}}}{R^{\pm}} W \left[\frac{I_{\text{0L,R}} R^{\pm}}{\eta_{\text{L,R}} V_{\text{T}}} \exp\left(\frac{|V| + I_{\text{0L,R}} R^{\pm}}{\eta_{\text{L,R}} V_{\text{T}}} \right) \right] \mp I_{\text{0L,R}} \tag{3}$$

where W is the Lambert function, i.e., the solution of the transcendental equation $W(x) \exp(W(x)) = x$. As discussed in a previous work,[55] a first-order correction term $R^{\pm} = R_0^{\pm} + R_1^{\pm} |V|$ resulting in a voltage-dependent resistance needs to be introduced in the model to account for the interface states at the contacts. It is important to remark that expression (3) considers different parameters for the two metal–insulator interfaces, thus allowing the model to represent both symmetric and asymmetric contact device configurations. Though this heuristic approximation provides a simple analytic treatment of the conduction problem, a more comprehensive and accurate solution can be found by directly solving the conduction characteristics of the combined devices using a circuit simulator, as presented later in Section 2.2 and described in detail in the Experimental Section.

Experimental data and modeling of a representative $I-V$ characteristic using (3) in an extended voltage range for a single NW device contacted by symmetric Pt electrodes is reported in Figure 2a. As can be seen, the $I-V$ characteristics exhibit a sigmoidal-like shape, in which the linear behavior can only be detected in a small voltage span around 0 V, while current saturation is reached for larger applied voltages. This behavior is a consequence of the current limitation imposed by the inverse saturation currents of the diode. Notably, it can be observed that the proposed model closely agrees with the experimental curve in the whole voltage range of analysis. Instead, Figure 2b reports experimental data and modeling results for a typical $I-V$ characteristic in an extended voltage range of an asymmetrically contacted ZnO NW with Pt and Ag electrodes. In this case, it can be observed that the $I-V$ characteristic shows, besides a rectifying behavior with negligible current flowing through the device when the Ag/ZnO interface is inversely biased, a tendency to reach the current saturation regime when the Ag/ZnO interface is positively biased. Also in this case, experimental data are well interpolated by modeling. Finally, as reported in Figure 2c, devices symmetrically contacted with Ag show a negligible electronic conductance (not modeled) even when stimulated in an extended voltage range. These results show that electronic transport in NW-based memristive cells in the pristine state can be well represented by the physics-based model described by eq 3. In particular, the close agreement between the thermionic emission model and the experimental data is testified by the low values assumed for the ideality factors (approximately from 1 to 2). With these values, NW resistances in the range of tens of MΩ to a few MΩ were found, but this strongly depends also on the considered saturation currents.

So far, the reported results demonstrate that the metal−insulator interface in electrochemical metallization memories can be used to regulate the electronic conductivity of the memristive cell in the pristine state. In particular, the electronic conduction in NW-based cells is observed to be mainly controlled by the inversely biased junction. Indeed, the inversely biased junction acts as a blocking barrier that limits the overall electronic current flowing through the device. In single ZnO NW devices, results show a more pronounced blocking action of the Ag/ZnO junction with respect to the Pt/ZnO junction. This can be clearly seen from the data reported in Figure 2, where the current is negligible for all of the cases where the Ag/ZnO junction is inversely biased (refer to Figure 2b,c). On the other hand, an inversely biased Pt/ZnO junction results in a nonnegligible saturation current that was observed to be in the range of hundreds of nA (refer to Figure 2a,b). It is worth noticing that a higher Schottky barrier is theoretically expected from the Schottky−Mott rule at the Pt/ZnO junction as a consequence of the higher Pt work function (5.12 eV) compared to the Ag work function (4.26 eV). However, the ideal Schottky−Mott rule does not consider possible chemical interactions occurring at the interfaces during the deposition of the metallic contacts.[56] For example, the formation of interfacial chemical bonds at the Pt/ZnO junction can be related to the formation of eutectics in between Pt and Zn,[57] causing a deviation from the ideal Schottky−Mott rule. It follows that the electronic conduction mechanism can be regulated by choosing contact materials with appropriate work functions and interface chemistry.

Metal−Insulator Interfaces and Memristive Behavior. In the NW-based electrochemical metallization cell previously discussed, ionic movement can be coupled to electronic transport depending on the operating conditions. Indeed, a positive voltage applied to an electrochemically active electrode causes the dissolution of atoms from the contact to form ions that start to migrate along the NW surface toward the counter electrode under the action of the applied electric field. As a consequence, a metallic filament bridging the two electrodes can be formed.[17] In single ZnO NW memristive cells, dissolution and migration of metal ions can be observed by positively biasing the Ag electrode due to the electrochemical activity of this metal, while the higher extraction barrier of Pt atoms from the contacts makes it an electrochemically inert electrode.[58] Therefore, ionic migration of Ag$^+$ ions with the consequent formation of an Ag conductive filament along the ZnO NW can be observed by biasing the Ag electrode in both asymmetric Pt/ZnO NW/Ag and symmetric Ag/ZnO NW/Ag devices. The investigation of the NW-based device through morphological and elemental analyses after resistive switching confirmed the ECM nature of the switching mechanism related to the formation of an Ag conductive filament along the ZnO NW surface (experimental evidence are reported in previous works[17,59−61]). The presence of Ag nanoclusters after resistive switching mainly accumulated near the Ag-biased electrode, as experimentally shown in a previous work,[25] suggests that the filament growth proceeds from the biased electrode and grows toward the counter electrode as discrete nanoclusters, as expected in resistive switching devices characterized by low cation mobility. Indeed, in low mobility, ions can pile and reach the critical nucleation conditions before reaching the counter electrode and filament growth can proceed by cluster displacement via repeated splitting−merging processes as discussed in ref 62. In this context, it is worth noticing also that previous works reported resistive switching in single NWs symmetrically contacted by electrochemical interelectrodes such as Ti or Ti/Au electrodes.[63−66] However, in these cases, the switching mechanism can be dominated by the TiO$_2$ interfacial layer formed at the Ti/ZnO interface, related to the higher affinity of Ti compared to Zn with O (the presence of this layer was experimentally revealed by transmission electron microscopy (TEM) analyses by Chiang et al.[66]). The presence of this layer can strongly impact the switching mechanism which in this case can be related to the migration of oxygen-related species at the ZnO/metal interface and not along the NW. In our case, no resistive switching was observed in Pt/ZnO NW/Pt devices.[17] The absence of resistive switching phenomena in Pt/ZnO NW/Pt symmetric devices testify that the switching mechanism in Ag-contacted devices is purely ECM and is not related to the migration of O species at the interface and/or along the NW, as expected in the valence change memory (VCM) mechanism.

After an initial assessment of the conductive filament generation by an electroforming step (details given in Figure S1), these devices exhibit resistive switching behavior because of the formation/rupture of the Ag conductive pathway. It is worth noticing that the electroforming voltage depends on the electrode spacing, where a substantial reduction of the voltage required for electroforming can be obtained by reducing the electrode spacing that, for the same applied voltage, results in a higher electric field.[17,25] In this context, the established metallic filamentary path along the NW surface provides an additional
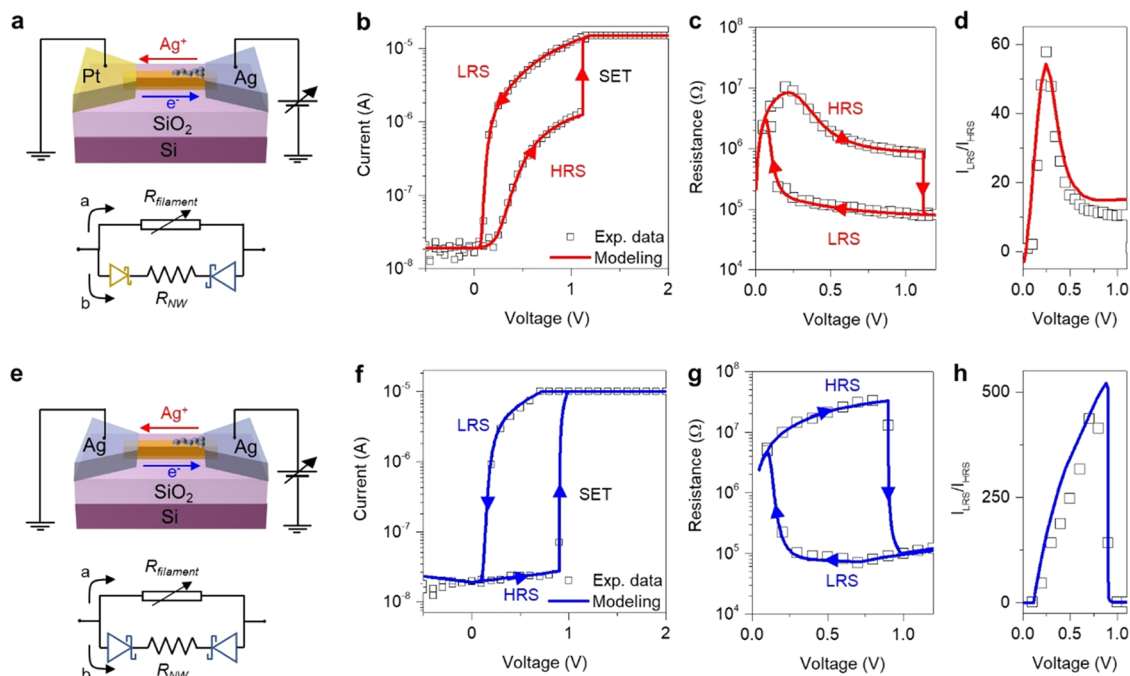
Figure 3. Experimental and modeling ionic transport properties and memristive behavior of single ZnO NW devices. (a) Schematization of the ZnO NW memristive cells with asymmetric Pt and Ag electrodes and its resistive switching mechanism based on the migration of Ag⁺ ions from the Ag electrode along the NW toward the Pt counter electrode under the action of the applied electric field. The equivalent circuital representation of the cell is represented by the back-to-back connected Schottky diodes in an asymmetric configuration with the NW series resistance R_{NW} (channel b), all in parallel with the variable resistance of the conductive filament (channel a). Experimental and modeled (b) memristive $I-V$ characteristics of a Pt/ZnO NW/Ag device, (c) corresponding $R-V$ characteristics showing the resistance window and (d) the I_{LRS}/I_{HRS} ratio as a function of the applied voltage. (e) Schematization of the ZnO NW memristive cells with symmetric Ag electrodes and its resistive switching mechanism based on the migration of Ag⁺ ions along the NWs under the action of the applied electric field. The equivalent circuital representation of the cell is represented by the back-to-back connected Schottky diodes in a symmetric configuration with the NW series resistance R_{NW} (channel b), all in parallel with the variable resistance of the conductive filament (channel a). Experimental and modeled (f) memristive $I-V$ characteristics of a Ag/ZnO NW/Ag device, (g) corresponding $R-V$ characteristics showing the resistance window and (h) the I_{LRS}/I_{HRS} ratio as a function of the applied voltage.

transport channel for electronic conduction. Indeed, when the conductive filament is established, electrons can flow parallel to the pathway consisting in the NW resistance and the Schottky interfaces previously discussed. The conductance properties of the filament-related electronic conduction channel are regulated by ionic dynamics underlying its formation/rupture under the action of the applied electric field. The hysteretic conduction characteristic and memory state dynamics resulting from the formation/rupture of the conductive filament can be modeled by a voltage-dependent rate balance equation that takes into account also short-term dynamics and volatility of the internal memory state related to the spontaneous relaxation of the Ag conductive filament.[67]

In this framework, the memory state resulting from filament dynamics can be described through the equation

$$\frac{dg}{dt} = k_p(1 - g) - k_d g \tag{4}$$

where g represents the memory state of the device in terms of its normalized conductance, while k_p and k_d are the potentiation and depression coefficients, respectively, which depend exponentially on the applied voltage as expected for diffusive ionic processes

$$k_{p,d} = k_{p0,d0} \exp(\eta_{p,d} V) \tag{5}$$

where η_p and η_d are the transition rates and k_{p0} and k_{d0} are the fitting constants. Equation 4 phenomenologically describes the

progressive arrival and departure of conducting species following a self-saturation process. Interestingly, the memory state eq 4 can be recursively solved by assuming a simulation timestep $\Delta t > 0$ as

$$g_t = \frac{\kappa_P}{\kappa_P + \kappa_D}[1 - e^{-(\kappa_P + \kappa_D)\Delta t}] + g_{t-1} e^{-(\kappa_P + \kappa_D)\Delta t} \tag{6}$$

Note that eq 6, which is not expressed as a continuous function of t, allows modeling the dynamics of the Ag conductive filament that regulates the evolution of the internal memory state of the memristive cell for an arbitrary stimulation voltage, provided Δt is small enough. Moreover, expression (6) captures the essence of hysteretic conduction since the current transport state (g_t) depends on the previous condition (g_{t-1}). For a constant applied voltage, eq 5 has analytic solution. Once the normalized conductance is found from eq 6, it can be straightforwardly used for computing the $I-V$ characteristics of the device. In this connection, different models can be considered for the electron transport, including, for example, a linear relationship $I \sim gV$ like in ref 67 or a more elaborated expression such as $I \sim g \sinh[\alpha(V - IR)]$ where α is a fitting constant and R is a series resistance, like the one used for the model curves in Figure 3. Notice that in this latter case, both for low voltages (HRS) and high currents (LRS), the $I-V$ curve becomes linear as well because of the role played by R. It is worth stressing that the model equations describe the formation/rupture of the filament without distinguishing the
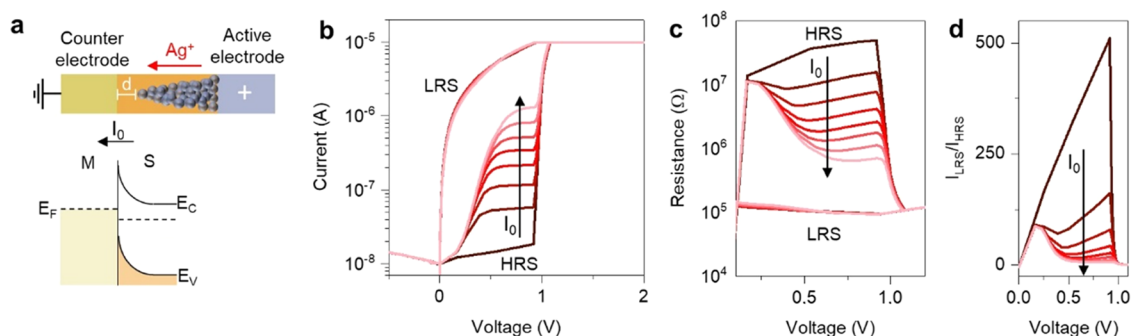
Figure 4. Effects of the metal−insulator interface at the counter electrode on the memristive characteristics. (a) Schematization of the ECM cell. Until the filament bridges the two electrodes (i.e., $d > 0$), the electronic conduction mechanism is dominated by the inversely polarized metal−semiconductor interface (M−S) and the current flowing into the device is determined by the saturation current at the Schottky interface. (b) Evolution of the $I−V$ memristive hysteretic loop, (c) corresponding $R−V$ characteristics and (d) the I_{LRS}/I_{HRS} ratio for ECM cells by progressively increasing (arrow direction) the saturation current I_0 at the metal−semiconductor interface of the counter electrode by modeling.

contributions of each individual physicochemical processes involved, such as redox processes, nucleation, diffusion, Butler−Volmer transport, field-accelerated transport, chemical dissolution, Gibbs−Thomson effect etc.

A schematization of the working principle of symmetric and asymmetric memristive cells with their corresponding electrical circuital representations and resistive switching characteristics are reported in Figure 3a−h, respectively. As a consequence of the coupling between ionics and electronics, asymmetric and symmetric single NW-based cells can be electrically modeled in a first approximation as a parallel combination of two conductive channels for electrons (Figure 3a,e), i.e., the metallic filament channel along the NW (channel a) and the ZnO semiconductor channel (channel b). In this framework, the internal cell voltage that can arise in asymmetrically contacted electrodes related to the nanobattery effect[68] is considered negligible. While the electron flow through channel a depends on the dynamics of the filament internal resistance state regulated by the applied voltage (in turn described by the memory state equation and its solution, eqs 4 and 6, the flow of electrons through channel b is regulated by the NW resistance itself and the Schottky barriers at the interfaces as described by the piecewise model with nonlinear series resistance correction, eq 3). Alternatively, a more comprehensive outcome can be obtained by representing and solving the whole system in a circuit simulator. The details of this numerical approach are provided in the Experimental Section of this work.

Experimental data and modeling results for representative $I−V$ resistive switching characteristics of asymmetrically contacted Pt/ZnO NW/Ag and symmetrically contacted Ag/ZnO NW/Ag devices are reported in Figure 3b,f, respectively (resistive switching characteristics of different devices from the same batch and devices from different batches are reported in Supporting Information, Figure S2). As can be observed, both devices exhibit hysteretic behavior related to the device switching from a high-resistance state (HRS) to a low-resistance state (LRS) in correspondence of the SET voltage. The switching characteristics are in both cases volatile as a consequence of the spontaneous dissolution of the Ag conductive filament, as previously discussed. While in this work we focus on volatile switching characteristics usually required for temporal processing of the input signal, a nonvolatile switching characteristic can be induced in both symmetric and asymmetric device configurations by properly

adjusting the operation conditions such as the compliance current level (details in Supporting Information, Figure S3). Note also that NW-based devices can be programmed by voltage pulses[17] (Supporting Information, Figure S4). Importantly, our modeling framework includes the effects of adding a current compliance to the experimental setup. As detailed in the Experimental Section, this limiting mechanism is modeled through the use of a variable resistor in series with the memristive structure. This allows to limit the current beyond the required maximum by adjusting the input voltage to the device, similarly to what happens in the experimental setup. During the time the current compliance is activated, the memory state of the device is allowed to evolve so that the emerging point of the $I−V$ characteristics when reducing the applied voltage (RESET) is no longer the same as the entrance point corresponding to the increasing voltage (SET). This is clearly seen, for example, in Figure 3f.

Despite similar switching characteristics, symmetric and asymmetric devices exhibit a different behavior in the HRS. Indeed, before SET events, the asymmetric device exhibits a sigmoidal-like behavior, while the symmetric device exhibits a negligible current flow. This means that in the HRS the device conductance is regulated by metal−ZnO interfaces, similarly to the pristine state case, where the inversely polarized junction at the counter electrode regulates the electron flow. Thus, in the HRS, where the filament is not formed, electrons flow mainly through the conduction channel b. Instead, similar behavior was observed in the LRS where the Ag conductive filament shorts the two electrodes in both symmetric and asymmetric configurations, and electrons flow mainly through the conduction channel a.

The different electronic conduction mechanisms in the HRS of asymmetric and symmetric devices lead to distinctive resistance window characteristics, as reported in Figure 3c,g, respectively. Due to the nonlinearity of the electronic conduction mechanism, here the HRS exhibits a maximum followed by a decrease as a function of the applied voltage. Instead, a monotonic increase of the HRS can be observed in symmetric devices, as a consequence of the blocking character of the reversely polarized Ag/ZnO contact. Thus, a wider resistance window can be observed in the $R−V$ loop of symmetrically contacted NWs. This in turn reflects in a higher ON/OFF ratio of the symmetrically contacted device, as it can be observed by comparing the LRS/HRS current ratio as a function of the voltage in the hysteresis loop for asymmetric
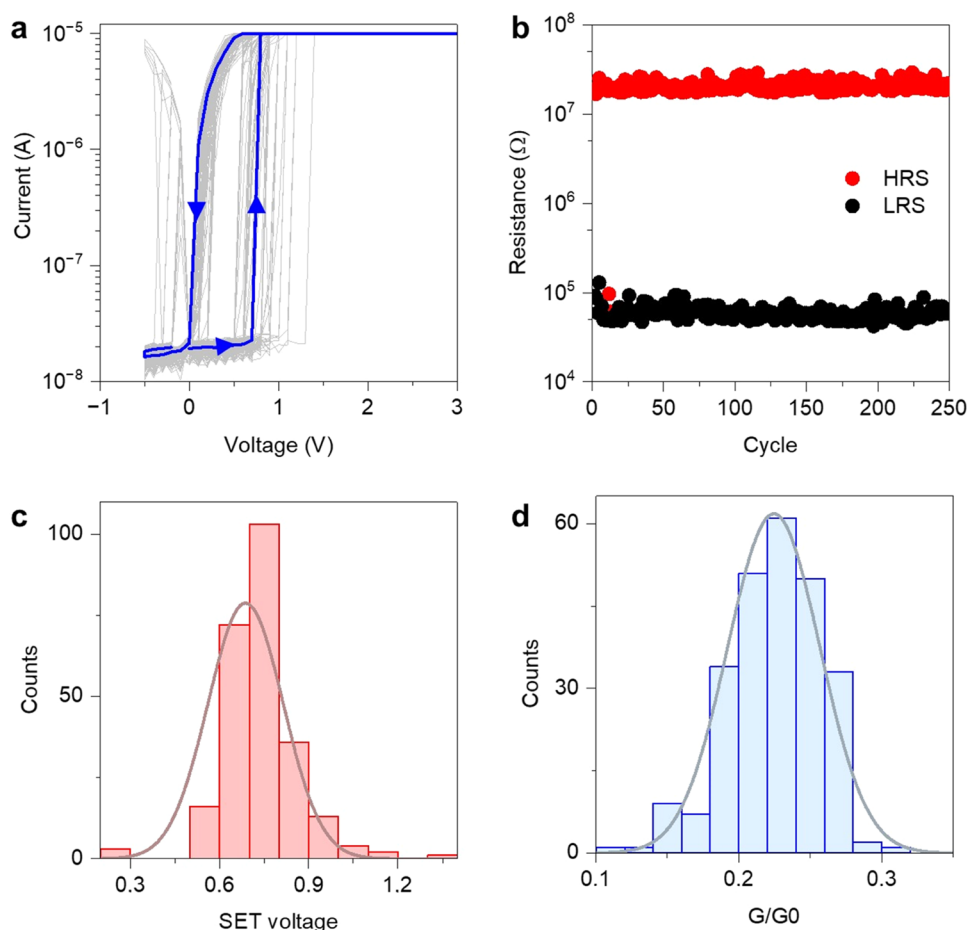
F

Figure 5. Memristive behavior of single ZnO NWs with symmetric Ag electrodes. (a) $I-V$ characteristics showing the resistive switching behavior over cycling. All of the 250 cycles are reported in light gray, while the median curve is reported in bold blue. (b) Endurance characteristics (read voltage of 0.4 V), (c) SET voltage distribution, and (d) distribution of conductance values in the LRS normalized by the fundamental quantum of conductance G_0. Data of panels (b−d) were extracted from 250 full-sweep cycles. The distributions in panels (c) and (d) are interpolated by normal distributions.

(Figure 3d) and symmetric (Figure 3h) devices. It is worth noticing also that, since the electronic transport properties in the HRS are mainly regulated by the reversely polarized Schottky junction at the metal/ZnO interface and not by the ZnO NW itself, no significant differences are expected at the Schottky barrier in the pristine state and after resistive switching loops. This hypothesis is supported by experimental data that shows a qualitative good overlapping of $I-V$ traces relative to the electroforming step before forming and the HRS of the device before SET (Supporting Information, Figure S5). In addition, these data also show no significant changes over cycling of the reversely polarized Schottky barrier that regulates the HRS, as testified by the good overlapping of $I-V$ traces in the HRS region over cycling.

More in general, these results indicate that the hysteretic memristive behavior can be tuned by a proper choice of the metal−insulator Schottky barrier at the counter electrode. Indeed, before the conductive filament bridges the two metallic electrodes, the reversely polarized Schottky interface at the counter electrode controls the flow of electrons in the device, where the electron flow corresponds to the saturation current of the reversely biased junction (Figure 4a). It turns out that, by progressively decreasing the saturation current of the junction through a clever choice of the electrode material, it is possible to enlarge not only the hysteretic loop but also the

corresponding resistance window as well as the LRS and HRS current ratio, as revealed by the model results reported in Figure 4b−d, respectively. In this context, it is important to remark that, as experimentally shown in the single NW device, the choice of the counter electrode material has to take into account both the theoretical Schottky barrier height expected by considering the counter electrode metal work function and the interface chemistry.

In single NWs, results show that the choice of Ag as a counter electrode allows to reduce the saturation current when reversely polarized, enhancing the ON/OFF switching ratio, as well as the separation of resistance states. In this framework, it is worth stressing that the switching characteristics of these symmetrically contacted devices with Ag electrodes are repeatable over cycling, as reported in Figure 5a. High stability and low dispersion of both HRS and LRS were observed in the endurance characteristics acquired during 250 full-sweep cycles, as reported in Figure 5b. In addition, a narrow dispersion of the SET voltage over cycling was observed. According to experiments, the SET voltage distribution reported in Figure 5c has a mean value of 0.69 V with a standard deviation of 0.13 V (details of the SET voltage as a function of cycling are reported in Supporting Information, Figure S6). Interestingly, the distribution of the device conductance over cycling in the LRS normalized with respect

to the fundamental quantum of conductance G_0 reported in Figure 5d shows that the device internal state of conductance is lower than G_0 (G/G_0 mean value of 0.22, standard deviation of 0.03). While values close to G_0 are expected when the filament size reaches the atomic scale favoring the formation of a quantum point contact,[69] values of $G < G_0$ mean that the formed filament does not allow the complete transmission of the electron wave packet. This corresponds to the tunneling regime through a subband. The effect can be explained by the formation of a noncontinuous metallic filament with the presence of an extremely narrow gap in the form of a broken-down filament and/or in the form of a sparse concentration of scatterers.

CONCLUSIONS

In conclusion, we have experimentally investigated and modeled the role played by metal−insulator interfaces in ECM cells, by considering single-crystalline ZnO NW-based devices as model systems. To this end, a number of symmetric and asymmetric device configurations have been considered, where Ag and Pt are exploited as representative electrochemically active and inert electrodes, respectively. A comparison of the electronic conduction properties of different devices highlights that the electron flow is mainly regulated by the metal−insulator interfaces. In this framework, experiments are in close agreement with the modeling of the memristive cells considered as two parallel conducting channels for electrons. The first channel, which dominates in the pristine state and in the HRS, is represented by back-to-back connected Schottky diodes in series with the NW resistance, while the conductance of the metallic filament channel, which dominates in the LRS, relies on the filament dynamics. Results show that the hysteretic characteristics can be modified by appropriate choice of the counter electrode metal that controls the flow of electrons in the HRS, as confirmed by experiments and modeling. In particular, a blocking counter electrode was observed to increase the resistance window, as reported in symmetrically contacted devices with Ag electrodes that are shown to exhibit also low SET voltages, together with reproducible switching characteristics. Besides highlighting the importance of the counter electrode in memristive devices, our results show that it is possible to cleverly design the hysteretic response of the memristive cell by controlling not only ionic transport properties but also the electronic aspect of the problem. To this aim, an appropriate choice of the contact materials should be done by taking into account not only the Schottky barrier height at the interface but also the interface chemistry. More in general, these results clearly point out that a rational design of memristive cells should rely on the selection of materials that properly regulate the electronic transport properties at the metal−insulator interfaces.

EXPERIMENTAL SECTION

Single NW Memristive Cell Fabrication. ZnO NWs were synthesized through low-pressure chemical vapor deposition by a self-seeding vapor−solid (VS) mechanism that involves the nucleation of ZnO and subsequent NW growth on a Pt substrate from the evaporation of a Zn source in an O_2 environment. The median NW length and diameter were assessed to be 1.6 μm and 100 nm, respectively. Each nanowire is a single crystal with high chemical purity and is characterized by a clean surface without any amorphous surface layers. Fabrication of single NW memristive cells was performed by combined optical and electron beam lithography (EBL), by connecting dispersed NWs on an insulating SiO_2 substrate

with a submillimetric prepatterned probe circuit. A two-step electron beam lithography and metal deposition were performed to obtain asymmetrically contacted NW-based memrsitive cells. A detailed description of the synthesis of ZnO NWs and fabrication steps of single NW devices can be found in our previous work.[46]

Electrical Characterization. Electrical characterization was performed in two-terminal configuration by a Keithley 6430 subfemtometer sourcemeter with a remote preamplifier, a Keithley 2636A, and a probe station. Electrical measurements of memristive devices in the pristine state in an extended voltage range (Figure 2) were performed on devices with a high electrode spacing to prevent ionic migration, thus avoiding resistive switching phenomena. All electrical measurements were performed in air at room temperature.

Modeling. A memristive cell model consisting of two back-to-back Schottky barriers in series with a nonlinear resistance (channel a) in combination with a parallel conducting channel exhibiting memristive properties (channel b) was implemented in LTspice (circuit simulator from Analog Devices). The script used for modeling is reported in Supporting Information, Figure S7 and contains five parts: parameter definition, memory state equation, current−voltage characteristic for the memristive device, current−voltage characteristic for the nano-wire, and auxiliary functions. The memristive behavior is based on an adaptation of the memdiode model for resistive switching devices reported in ref 70. The model includes the snapback effect and an internal series resistance. A schematic representation of the circuit used for modeling is reported in Supporting Information, Figure S8.

ASSOCIATED CONTENT

Supporting Information

The Supporting Information is available free of charge at https://pubs.acs.org/doi/10.1021/acsami.2c11022.

Typical electroforming characteristics of a single NW memristive cell by applying a positive bias to an electrochemically active Ag electrode (Figure S1); resistive switching behavior of different Ag/ZnO NW/ Pt devices from the same batch and from a different batch (Figure S2); nonvolatile resistive switching in symmetrically contacted ZnO NWs with Ag electrodes (Figure S3); resistive switching behavior of an Ag/ZnO NW/Pt device observed under voltage pulse stimulation (Figure S4); comparison of $I-V$ traces of electroforming and resistive switching cycles of an Ag/ZnO NW/PT device (Figure S5); SET voltage as a function of the switching cycle (Figure S6); script for modeling the memristive cell with two back-to-back Schottky barrier systems (Figure S7); and LTspice circuit representation (Figure S8) (PDF)

AUTHOR INFORMATION

Corresponding Authors

Gianluca Milano − *Advanced Materials Metrology and Life Sciences Division, INRiM (Istituto Nazionale di Ricerca Metrologica), 10135 Torino, Italy;* orcid.org/0000-0002-1983-6516; Email: g.milano@inrim.it

Carlo Ricciardi − *Department of Applied Science and Technology, Politecnico di Torino, 10129 Torino, Italy;* orcid.org/0000-0002-4703-7949; Email: carlo.ricciardi@polito.it

Authors

Enrique Miranda − *Departament d'Enginyeria Electrònica, Universitat Autònoma de Barcelona (UAB), 08193 Cerdanyola del Vallès, Spain*

Matteo Fretto − *Advanced Materials Metrology and Life Sciences Division, INRiM (Istituto Nazionale di Ricerca Metrologica), 10135 Torino, Italy*

Ilia Valov − *JARA—Fundamentals for Future Information Technology, 52425 Jülich, Germany; Peter-Grünberg-Institut (PGI 7), Forschungszentrum Jülich, 52425 Jülich, Germany;* ⊙ orcid.org/0000-0002-0728-7214

Complete contact information is available at:
https://pubs.acs.org/10.1021/acsami.2c11022

Notes

■ ACKNOWLEDGMENTS

■ REFERENCES

(1) Christensen, D. V.; Dittmann, R.; Linares-Barranco, B.; Sebastian, A.; Le Gallo, M.; Redaelli, A.; Slesazeck, S.; Mikolajick, T.; Spiga, S.; Menzel, S.; Valov, I.; Milano, G.; Ricciardi, C.; Liang, S.-J.; Miao, F.; Lanza, M.; Quill, T. J.; Keene, S. T.; Salleo, A.; Grollier, J.; Markovic, D.; Mizrahi, A.; Yao, P.; Yang, J. J.; Indiveri, G.; Strachan, J. P.; Datta, S.; Vianello, E.; Valentian, A.; Feldmann, J.; Li, X.; Pernice, W. H.; Bhaskaran, H.; Furber, S.; Neftci, E.; Scherr, F.; Maass, W.; Ramaswamy, S.; Tapson, J.; Panda, P.; Kim, Y.; Tanaka, G.; Thorpe, S.; Bartolozzi, C.; Cleland, T. A.; Posch, C.; Liu, S.-C.; Panuccio, G.; Mahmud, M.; Mazumder, A. N.; Hosseini, M.; Mohsenin, T.; Donati, E.; Tolu, S.; Galeazzi, R.; Christensen, M. E.; Holm, S.; Ielmini, D.; Pryds, N. 2022 Roadmap on Neuromorphic Computing and Engineering. *Neuromorphic Comput. Eng.* **2022**, *2*, No. 022501.

(2) Berggren, K.; Xia, Q.; Likharev, K. K.; Strukov, D. B.; Jiang, H.; Mikolajick, T.; Querlioz, D.; Salinga, M.; Erickson, J. R.; Pi, S.; Xiong, F.; Lin, P.; Li, C.; Chen, Y.; Xiong, S.; Hoskins, B. D.; Daniels, M. W.; Madhavan, A.; Liddle, J. A.; McClelland, J. J.; Yang, Y.; Rupp, J.; Nonnenmann, S. S.; Cheng, K.-T.; Gong, N.; Lastras-Montaño, M. A.; Talin, A. A.; Salleo, A.; Shastri, B. J.; de Lima, T. F.; Prucnal, P.; Tait, A. N.; Shen, Y.; Meng, H.; Roques-Carmes, C.; Cheng, Z.; Bhaskaran, H.; Jariwala, D.; Wang, H.; Shainline, J. M.; Segall, K.; Yang, J. J.; Roy, K.; Datta, S.; Raychowdhury, A. Roadmap on Emerging Hardware and Technology for Machine Learning. *Nanotechnology* **2021**, *32*, No. 012002.

(3) Li, H.; Wang, S.; Zhang, X.; Wang, W.; Yang, R.; Sun, Z.; Feng, W.; Lin, P.; Wang, Z.; Sun, L.; Yao, Y. Memristive Crossbar Arrays for Storage and Computing Applications. *Adv. Intell. Syst.* **2021**, *3*, No. 2100017.

(4) Ielmini, D.; Pedretti, G. Device and Circuit Architectures for In-Memory Computing. *Adv. Intell. Syst.* **2020**, *2*, No. 2000040.

(5) Xia, Q.; Yang, J. J. Memristive Crossbar Arrays for Brain-Inspired Computing. *Nat. Mater.* **2019**, *18*, 309−323.

(6) Tang, J.; Yuan, F.; Shen, X.; Wang, Z.; Rao, M.; He, Y.; Sun, Y.; Li, X.; Zhang, W.; Li, Y.; Gao, B.; Qian, H.; Bi, G.; Song, S.; Yang, J. J.; Wu, H. Bridging Biological and Artificial Neural Networks with Emerging Neuromorphic Devices: Fundamentals, Progress, and Challenges. *Adv. Mater.* **2019**, *31*, No. 1902761.

(7) Yang, J. Q.; Wang, R.; Ren, Y.; Mao, J. Y.; Wang, Z. P.; Zhou, Y.; Han, S. T. Neuromorphic Engineering: From Biological to Spike-Based Hardware Nervous Systems. *Adv. Mater.* **2020**, *32*, No. 2003610.

(8) Wang, Z.; Wu, H.; Burr, G. W.; Hwang, C. S.; Wang, K. L.; Xia, Q.; Yang, J. J. Resistive Switching Materials for Information Processing. *Nat. Rev. Mater.* **2020**, *5*, 173−195.

(9) Lanza, M.; Sebastian, A.; Lu, W. D.; le Gallo, M.; Chang, M.-F.; Akinwande, D.; Puglisi, F. M.; Alshareef, H. N.; Liu, M.; Roldan, J. B. Memristive Technologies for Data Storage, Computation, Encryption, and Radio-Frequency Communication. *Science* **2022**, *376*, No. eabj9979.

(10) Xiong, X.; Xiong, F.; Tian, H.; Wang, Z.; Wang, Y.; Tao, R.; Klausen, L. H.; Dong, M. Ultrathin Anion Conductors Based Memristor. *Adv. Electron. Mater.* **2022**, *8*, No. 2100845.

(11) Khot, A. C.; Dongale, T. D.; Park, J. H.; Kesavan, A. V.; Kim, T. G. Ti_3C_2-Based MXene Oxide Nanosheets for Resistive Memory and Synaptic Learning Applications. *ACS Appl. Mater. Interfaces* **2021**, *13*, 5216−5227.

(12) Dittmann, R.; Strachan, J. P. Redox-Based Memristive Devices for New Computing Paradigm. *APL Mater.* **2019**, *7*, No. 110903.

(13) Waser, R.; Dittmann, R.; Staikov, G.; Szot, K. Redox-Based Resistive Switching Memories-Nanoionic Mechanisms, Prospects, and Challenges. *Adv. Mater.* **2009**, *21*, 2632−2663.

(14) Waser, R.; Aono, M. Nanoionics-Based Resistive Switching Memories. *Nat. Mater.* **2007**, *6*, 833−840.

(15) Valov, I.; Waser, R.; Jameson, J. R.; Kozicki, M. N. Electrochemical Metallization Memories—Fundamentals, Applications, Prospects. *Nanotechnology* **2011**, *22*, No. 289502.

(16) Wang, W.; Wang, M.; Ambrosi, E.; Bricalli, A.; Laudato, M.; Sun, Z.; Chen, X.; Ielmini, D. Surface Diffusion-Limited Lifetime of Silver and Copper Nanofilaments in Resistive Switching Devices. *Nat. Commun.* **2019**, *10*, No. 81.

(17) Milano, G.; Luebben, M.; Ma, Z.; Dunin-Borkowski, R.; Boarino, L.; Pirri, C. F.; Waser, R.; Ricciardi, C.; Valov, I. Self-Limited Single Nanowire Systems Combining All-in-One Memristive and Neuromorphic Functionalities. *Nat. Commun.* **2018**, *9*, No. 5151.

(18) Ohno, T.; Hasegawa, T.; Tsuruoka, T.; Terabe, K.; Gimzewski, J. K.; Aono, M. Short-Term Plasticity and Long-Term Potentiation Mimicked in Single Inorganic Synapses. *Nat. Mater.* **2011**, *10*, 591−595.

(19) Milano, G.; Pedretti, G.; Montano, K.; Ricci, S.; Hashemkhani, S.; Boarino, L.; Ielmini, D.; Ricciardi, C. In Materia Reservoir Computing with a Fully Memristive Architecture Based on Self-Organizing Nanowire Networks. *Nat. Mater.* **2022**, *21*, 195−202.

(20) Zhong, Y.; Tang, J.; Li, X.; Gao, B.; Qian, H.; Wu, H. Dynamic Memristor-Based Reservoir Computing for High-Efficiency Temporal Signal Processing. *Nat. Commun.* **2021**, *12*, No. 408.

(21) Midya, R.; Wang, Z.; Asapu, S.; Zhang, X.; Rao, M.; Song, W.; Zhuo, Y.; Upadhyay, N.; Xia, Q.; Yang, J. J. Reservoir Computing Using Diffusive Memristors. *Adv. Intell. Syst.* **2019**, *1*, No. 1900084.

(22) Moon, J.; Ma, W.; Shin, J. H.; Cai, F.; Du, C.; Lee, S. H.; Lu, W. D. Temporal Data Classification and Forecasting Using a Memristor-Based Reservoir Computing System. *Nat. Electron.* **2019**, *2*, 480−487.

(23) Milano, G.; Pedretti, G.; Fretto, M.; Boarino, L.; Benfenati, F.; Ielmini, D.; Valov, I.; Ricciardi, C. Brain-Inspired Structural Plasticity through Reweighting and Rewiring in Multi-Terminal Self-Organizing Memristive Nanowire Networks. *Adv. Intell. Syst.* **2020**, *2*, No. 2000096.

(24) Milano, G.; Porro, S.; Valov, I.; Ricciardi, C. Recent Developments and Perspectives for Memristive Devices Based on Metal Oxide Nanowires. *Adv. Electron. Mater.* **2019**, *5*, No. 1800909.

(25) Milano, G.; Raffone, F.; Luebben, M.; Boarino, L.; Cicero, G.; Valov, I.; Ricciardi, C. Water-Mediated Ionic Migration in Memristive Nanowires with a Tunable Resistive Switching Mechanism. *ACS Appl. Mater. Interfaces* **2020**, *12*, 48773−48780.

(26) Nagashima, K.; Yanagida, T.; Oka, K.; Kanai, M.; Klamchuen, A.; Kim, J.-S.; Park, B. H.; Kawai, T. Intrinsic Mechanism of Memristive Switching. *Nano Lett.* **2011**, *11*, 2114−2118.

(27) Nagashima, K.; Yanagida, T.; Oka, K.; Taniguchi, M.; Kawai, T.; Kim, J. S.; Park, B. H. Resistive Switching Multistate Nonvolatile Memory Effects in a Single Cobalt Oxide Nanowire. *Nano Lett.* **2010**, *10*, 1359−1363.

(28) Oka, K.; Yanagida, T.; Nagashima, K.; Kanai, M.; Kawai, T.; Kim, J. S.; Park, B. H. Spatial Nonuniformity in Resistive-Switching Memory Effects of Nio. *J. Am. Chem. Soc.* **2011**, *133*, 12482−12485.

(29) Oka, K.; Yanagida, T.; Nagashima, K.; Tanaka, H.; Kawai, T. Nonvolatile Bipolar Resistive Memory Switching in Single Crystalline Nio Heterostructured Nanowires. *J. Am. Chem. Soc.* **2009**, *131*, 3434−3435.

(30) Bandopadhyay, K.; Prajapati, K. N.; Mitra, J. Resistive Switching in Individual ZnO Nanorods: Delineating the Ionic Current by Photo-Stimulation. *Nanotechnology* **2018**, *29*, No. 105701.

(31) Valov, I.; Lu, W. D. Nanoscale Electrochemistry Using Dielectric Thin Films as Solid Electrolytes. *Nanoscale* **2016**, *8*, 13828−13837.

(32) Lübben, M.; Valov, I. Active Electrode Redox Reactions and Device Behavior in ECM Type Resistive Switching Memories. *Adv. Electron. Mater.* **2019**, *5*, No. 1800933.

(33) Liu, Q.; Sun, J.; Lv, H.; Long, S.; Yin, K.; Wan, N.; Li, Y.; Sun, L.; Liu, M. Real-Time Observation on Dynamic Growth/Dissolution of Conductive Filaments in Oxide-Electrolyte-Based ReRAM. *Adv. Mater.* **2012**, *24*, 1844−1849.

(34) Celano, U.; Goux, L.; Belmonte, A.; Opsomer, K.; Franquet, A.; Schulze, A.; Detavernier, C.; Richard, O.; Bender, H.; Jurczak, M.; Vandervorst, W. Three-Dimensional Observation of the Conductive Filament in Nanoscaled Resistive Memory Devices. *Nano Lett.* **2014**, *14*, 2401−2406.

(35) Yang, Y.; Gao, P.; Gaba, S.; Chang, T.; Pan, X.; Lu, W. Observation of Conducting Filament Growth in Nanoscale Resistive Memories. *Nat. Commun.* **2012**, *3*, No. 732.

(36) Sun, W.; Gao, B.; Chi, M.; Xia, Q.; Yang, J. J.; Qian, H.; Wu, H. Understanding Memristive Switching via in Situ Characterization and Device Modeling. *Nat. Commun.* **2019**, *10*, No. 3453.

(37) Lübben, M.; Cüppers, F.; Mohr, J.; von Witzleben, M.; Breuer, U.; Waser, R.; Neumann, C.; Valov, I. Design of Defect-Chemical Properties and Device Performance in Memristive Systems. *Sci. Adv.* **2020**, *6*, No. eaaz9079.

(38) Valov, I.; Tsuruoka, T. Effects of Moisture and Redox Reactions in VCM and ECM Resistive Switching Memories. *J. Phys. D: Appl. Phys.* **2018**, *51*, No. 413001.

(39) Messerschmitt, F.; Kubicek, M.; Rupp, J. L. M. How Does Moisture Affect the Physical Property of Memristance for Anionic-Electronic Resistive Switching Memories? *Adv. Funct. Mater.* **2015**, *25*, 5117−5125.

(40) Milano, G.; Luebben, M.; Laurenti, M.; Boarino, L.; Ricciardi, C.; Valov, I. Structure-Dependent Influence of Moisture on Resistive Switching Behavior of ZnO Thin Films. *Adv. Mater. Interfaces* **2021**, *8*, No. 2100915.

(41) Milano, G.; Luebben, M.; Laurenti, M.; Porro, S.; Bejtka, K.; Bianco, S.; Breuer, U.; Boarino, L.; Valov, I.; Ricciardi, C. Ionic Modulation of Electrical Conductivity of ZnO Due to Ambient Moisture. *Adv. Mater. Interfaces* **2019**, *6*, No. 1900803.

(42) Chen, S.; Valov, I. Design of Materials Configuration for Optimizing Redox-Based Resistive Switching Memories. *Adv. Mater.* **2022**, *34*, No. 2105022.

(43) Valov, I. Interfacial Interactions and Their Impact on Redox-Based Resistive Switching Memories (ReRAMs). *Semicond. Sci. Technol.* **2017**, *32*, No. 093006.

(44) Cho, D.-Y.; Luebben, M.; Wiefels, S.; Lee, K.-S.; Valov, I. Interfacial Metal−Oxide Interactions in Resistive Switching Memories. *ACS Appl. Mater. Interfaces* **2017**, *9*, 19287−19295.

(45) Tappertzhofen, S.; Valov, I.; Tsuruoka, T.; Hasegawa, T.; Waser, R.; Aono, M. Generic Relevance of Counter Charges for Cation-Based Nanoscale Resistive Switching Memories. *ACS Nano* **2013**, *7*, 6396−6402.

(46) Milano, G.; Boarino, L.; Valov, I.; Ricciardi, C. Memristive Devices Based on Single ZnO Nanowires—from Material Synthesis to Neuromorphic Functionalities. *Semicond. Sci. Technol.* **2022**, *37*, No. 034002.

(47) Milano, G.; Porro, S.; Ali, M. Y.; Bejtka, K.; Bianco, S.; Beccaria, F.; Chiolerio, A.; Pirri, C. F.; Ricciardi, C. Unravelling Resistive Switching Mechanism in ZnO NW Arrays: The Role of the Polycrystalline Base Layer. *J. Phys. Chem. C* **2018**, *122*, 866−874.

(48) Porro, S.; Risplendi, F.; Cicero, G.; Bejtka, K.; Milano, G.; Rivolo, P.; Jasmin, A.; Chiolerio, A.; Pirri, C. F.; Ricciardi, C. Multiple Resistive Switching in Core−Shell ZnO Nanowires Exhibiting Tunable Surface States. *J. Mater. Chem. C* **2017**, *5*, 10517−10523.

(49) Yin, H.; Wang, Q.; Geburt, S.; Milz, S.; Ruttens, B.; Degutis, G.; D'Haen, J.; Shan, L.; Punniyakoti, S.; D'Olieslaeger, M.; Wagner, P.; Ronning, C.; Boyen, H.-G. Controlled Synthesis of Ultrathin ZnO Nanowires Using Micellar Gold Nanoparticles as Catalyst Templates. *Nanoscale* **2013**, *5*, 7046.

(50) Zhang, Z.; Yao, K.; Liu, Y.; Jin, C.; Liang, X.; Chen, Q.; Peng, L.-M. Quantitative Analysis of Current-Voltage Characteristics of Semiconducting Nanowires: Decoupling of Contact Effects. *Adv. Funct. Mater.* **2007**, *17*, 2478−2489.

(51) Milano, G.; D'Ortenzi, L.; Bejtka, K.; Ciubini, B.; Porro, S.; Boarino, L.; Ricciardi, C. Metal−Insulator Transition in Single Crystalline ZnO Nanowires. *Nanotechnology* **2021**, *32*, No. 185202.

(52) Janotti, A.; Van de Walle, C. G. Fundamentals of Zinc Oxide as a Semiconductor. *Rep. Prog. Phys.* **2009**, *72*, No. 126501.

(53) Chiu, S.-P.; Lin, Y.-H.; Lin, J.-J. Electrical Conduction Mechanisms in Natively Doped ZnO Nanowires. *Nanotechnology* **2009**, *20*, No. 015203.

(54) Tsai, L.-T.; Chiu, S.-P.; Lu, J. G.; Lin, J.-J. Electrical Conduction Mechanisms in Natively Doped ZnO Nanowires (II). *Nanotechnology* **2010**, *21*, No. 145202.

(55) Miranda, E.; Milano, G.; Ricciardi, C. Compact Modeling of the I-V Characteristics of ZnO Nanowires Including Nonlinear Series Resistance Effects. *IEEE Trans. Nanotechnol.* **2020**, *19*, 297−300.

(56) Liu, Y.; Guo, J.; Zhu, E.; Liao, L.; Lee, S.; Ding, M.; Shakir, I.; Gambin, V.; Huang, Y.; Duan, X. Approaching the Schottky−Mott Limit in van Der Waals Metal−Semiconductor Junctions. *Nature* **2018**, *557*, 696−700.

(57) Brillson, L. J.; Lu, Y. ZnO Schottky Barriers and Ohmic Contacts. *J. Appl. Phys.* **2011**, *109*, No. 121301.

(58) Raffone, F.; Cicero, G. Does Platinum Play a Role in the Resistance Switching of ZnO Nanowire-Based Devices? *Solid State Ionics* **2017**, *299*, 93−95.

(59) Yang, Y.; Zhang, X.; Gao, M.; Zeng, F.; Zhou, W.; Xie, S.; Pan, F. Nonvolatile Resistive Switching in Single Crystalline ZnO Nanowires. *Nanoscale* **2011**, *3*, 1917.

(60) Qi, J.; Huang, J.; Paul, D.; Ren, J.; Chu, S.; Liu, J. Current Self-Complianced and Self-Rectifying Resistive Switching in Ag-Electroded Single Na-Doped ZnO Nanowires. *Nanoscale* **2013**, *5*, 2651.

(61) Milano, G.; Boarino, L.; Ricciardi, C. Junction Properties of Single ZnO Nanowires with Asymmetrical Pt and Cu Contacts. *Nanotechnology* **2019**, *30*, No. 244001.

(62) Yang, Y.; Gao, P.; Li, L.; Pan, X.; Tappertzhofen, S.; Choi, S.; Waser, R.; Valov, I.; Lu, W. D. Electrochemical Dynamics of Nanoscale Metallic Inclusions in Dielectrics. *Nat. Commun.* **2014**, *5*, No. 4232.

(63) Zhang, R.; Pang, W.; Zhang, Q.; Chen, Y.; Chen, X.; Feng, Z.; Yang, J.; Zhang, D. Enhanced Non-Volatile Resistive Switching in Suspended Single-Crystalline ZnO Nanowire with Controllable Multiple States. *Nanotechnology* **2016**, *27*, No. 315203.

(64) Lai, Y.; Xin, P.; Cheng, S.; Yu, J.; Zheng, Q. Plasma Enhanced Multistate Storage Capability of Single ZnO Nanowire Based Memory. *Appl. Phys. Lett.* **2015**, *106*, No. 031603.

(65) Lai, Y.; Qiu, W.; Zeng, Z.; Cheng, S.; Yu, J.; Zheng, Q. Resistive Switching of Plasma−Treated Zinc Oxide Nanowires for Resistive Random Access Memory. *Nanomaterials* **2016**, *6*, No. 16.

(66) Chiang, Y. D.; Chang, W. Y.; Ho, C. Y.; Chen, C. Y.; Ho, C. H.; Lin, S. J.; Wu, T. B.; He, J. H. Single-ZnO-Nanowire Memory. *IEEE Trans. Electron Devices* **2011**, *58*, 1735−1740.

(67) Miranda, E.; Milano, G.; Ricciardi, C. Modeling of Short-Term Synaptic Plasticity Effects in ZnO Nanowire-Based Memristors Using a Potentiation-Depression Rate Balance Equation. *IEEE Trans. Nanotechnol.* **2020**, *19*, 609−612.

(68) Valov, I.; Linn, E.; Tappertzhofen, S.; Schmelzer, S.; van den Hurk, J.; Lentz, F.; Waser, R. Nanobatteries in Redox-Based Resistive Switches Require Extension of Memristor Theory. *Nat. Commun.* **2013**, *4*, No. 1771.

(69) Milano, G.; Aono, M.; Boarino, L.; Celano, U.; Hasegawa, T.; Kozicki, M.; Majumdar, S.; Menghini, M.; Miranda, E.; Ricciardi, C.; Tappertzhofen, S.; Terabe, K.; Valov, I. Quantum Conductance in Memristive Devices: Fundamentals, Developments, and Applications. *Adv. Mater.* **2022**, *34*, No. 2201248.

(70) Aguirre, F. L.; Suñé, J.; Miranda, E. SPICE Implementation of the Dynamic Memdiode Model for Bipolar Resistive Switching Devices. *Micromachines* **2022**, *13*, 330.